Aquat. Living Resour. 2021, 34, 15
© EDP Sciences 2021
https://doi.org/10.1051/alr/2021015

Aquatic Living Resources
Available online at:
www.alr-journal.org

Research Article

Mapping and estimating harvest potential of seaweed culture using Worldview-2 Satellite images: a case study in Nusa Lembongan, Bali – Indonesia

Indra Pratama* and Hatim Albasri

Center for Fisheries Research – Ministry of Marine Affairs and Fisheries, Jl. Raya Ragunan No. 20, Pasar Minggu, Jakarta 12540, Indonesia

Received 11 July 2020 / Accepted 18 May 2021

Handling Editor: Ellen Kenchington

Abstract – Unreliable information on harvest potential is a persistent challenge for the Indonesian government and industry alike to manage an efficient supply chain of seaweed raw material. The use of remote sensing technology to assess seaweed harvest potential has been scarcely available in the literature. This current research aimed at estimating the harvest potential of seaweed *Kappaphycus alvarezii* through remote sensing using supervised classification with maximum likelihood (MLC) and contextual editing (CE) methods. This research evaluated the capabilities of different band combinations along with depth invariant index (DII) to enhance the remote sensing accuracy in estimating seaweed harvest potential. The seaweed classification using Worldview-2 imagery was compared with the in-situ references (ground-truthing). The potential data bias resulted from different imagery acquisition timestamps with the in-situ measurement was kept minimal as both data time stamps were ten days apart and within the same seaweed culture cycle. The average dry weight of all seaweed samples collected during the research was 924 ± 278.91 g/m^2 with culture ages between 1 and 40 days. The classification results based on MLC+CE with a 5-band combination method without DII showed a better correlation and closer fit with the in-situ references compared to the other methods, with an overall accuracy of 79.05% and Tau coefficient value of 0.75. The estimated total harvest potential based on the combined seaweed classes was 531.26 ± 250.29 tons dry weight.

Keywords: *Kappaphycus alvarezii* / Worldview-2 / seaweed / biomass

1 Introduction

Seaweed remains the leading aquaculture product exported by several Southeast Asian countries including Indonesia (Sievanen et al., 2005; Benfield et al., 2007; Zamroni and Yamao, 2011; Andréfouët et al., 2018). In Indonesia, small-scale seaweed farmings are conducted in a combined areas larger than Luxembourg and directly employs more than half-million seaweed farmers (MMAF, 2015). In 2016, 11.6 million tons of seaweed was produced by Indonesian farmers (FAO, 2018), an increase of almost twofold from the 2012 production (FAO, 2014). The total farming areas were under 25% of the total potential area of 1.12 million ha (Zamroni and Yamao, 2011) and have stayed relatively constant up to 2018 (MMAF, 2019). Seaweed *Kappaphycus* and *Eucheuma* dominates most of the Indonesian seaweed products (Sievanen et al., 2005). However, other genera such as *Gracillaria* (Zamroni and Yamao, 2011) and *Caulerpa* (Perryman et al., 2017) are gaining popularity among Indonesia's seaweed farmers. The importance of seaweed in generating significant additional income has a positive effect on fish resource management. For example, reduced fishing pressures on wild fish stock were evident in many remote small-island waters due to fishermen shifting to seaweed farming (Sievanen et al., 2005; Zamroni and Yamao, 2011; Andréfouët et al., 2018).

However, seaweed production in Indonesia is difficult to measure or predict due to the remoteness of most seaweed production centers within the Indonesian archipelago. The geographical disadvantage and limited communication infrastructure in these remote areas have resulted in data distortion or data loss along the seaweed market chains. As a result, seaweed industries regularly experience supply shortages and uncertainties due to failures to predict seaweed biomass

*Corresponding author: indrapratama@kkp.go.id

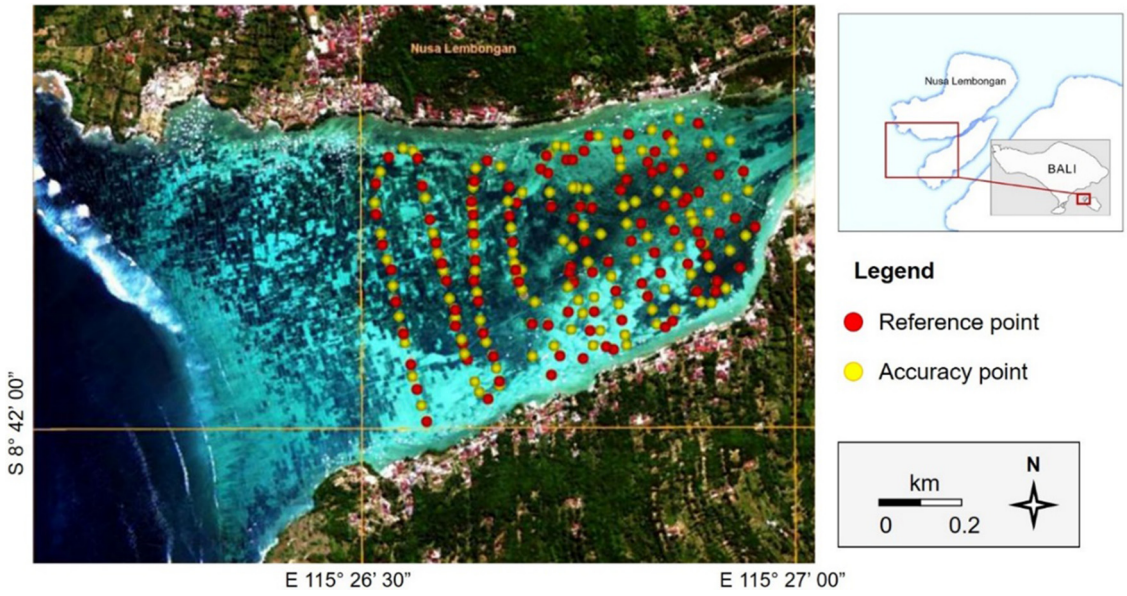

Fig. 1. Study area in Nusa Lembongan Island.

production (Mulyati and Geldermann, 2017). In most cases, the industries desperately sourced seaweed supplies from other producers or areas at a higher price (Sarinah and Djatna, 2015).

The Indonesian government also faces difficulties to sustainably develop the industry due to the lack of reliable data regarding the harvest potential of seaweed (Wright, 2017). The ability to efficiently map the distribution of existing and seasonally productive areas and determine new potential suitable sites were quite challenging. These issue contributes to inaccuracies in predicting the harvest potential of Indonesian seaweed. Solving these inaccuracies are essential in reducing the risk of supply uncertainties in the seaweed market chain and the future development of seaweed aquaculture.

Using remote sensing in mapping of locations and potential harvest of seaweed is an efficient method in terms of cost, time, and resource use. It also has a greater coverage compared to in-situ survey sampling. The current sensor and processing technologies of remote sensing can determine various characteristics of vegetation such as species variation, biomass distribution, and chemical compounds (Silva et al., 2008). However, remote sensing technology has some limitations to accurately estimate certain submerged vegetations and differentiate each of them due to spatial resolution, cost, and cloud cover (Stekoll et al., 2006; Silva et al., 2008). For example, the use of Landsat 7 ETM had a 50% greater area measurement compared to the in-situ measurement of kelp canopy area in South Alaska (Stekoll et al., 2006). Fortunately, remote sensing accuracy to estimate aquatic vegetation biomass can be increased by up to 80% through improvement of ground-truthing technique, spectral comparison, satellite resolution and sensor used, classification procedure, and algorithm modification (Green et al., 2000; Silva et al., 2008). Several studies have been carried out with the main objective to improve identification technique of objects submerged in shallow water through modification and development of image processing algorithm with promising results and high accuracies (Tassan, 1996; Stekoll et al., 2006; Andréfouët et al., 2004, 2017; Sagawa et al., 2010; Kanno and Tanaka, 2012; Wouthuyzen et al., 2016; Setyawidati et al., 2017, 2018a,b).

One particular method that is of interest to this research is water column correction, also known as depth invariant index (DII) developed by Lyzenga (1981). DII incorporates depth information into the spectral classification method to reduce the effect of water column on spectral reflectances (Ackleson and Klemas, 1987). The combination of DII and spectral classification methods such as Maximum Likelihood Classification (MLC) could theoretically improve the prediction of seaweed harvestable biomass. Mumby et al. (1998) proved that applying the water column correction method in the initial stage of image classification could significantly improve map accuracies compared with only using the original bands. Furthermore, combining DII with contextual editing could improved the classification results compared to simply use the original bands. Despite the classification results were not always significant, this combined approach had collectively produced higher map accuracy than applying DII or contextual editing alone (Mumby et al., 1998). For the aforementioned reasons, this research aimed at evaluating the effects of incorporating DII into the multispectral maximum likelihood classification with contextual editing in estimating seaweed *Kappaphycus alvarezii* harvestable biomass.

2 Methods

2.1 Study area

The selected study site was a *K. alvarezii* seaweed farming area located in a coastal shallow water at southernmost part of Nusa Lembongan, Klungkung Regency, Bali, Indonesia (Fig. 1). The seaweed farming was carried out traditionally using a bottom long-line method where rope lines of 50–100 m long were stretched between two bamboo poles. Seaweed

seeds of around 50 g were tied along the ropes at a distance of 15–20 cm and harvested after 40 to 45 days (Sulistijo, 2002; Anggadiredja et al., 2006). Seawater clarity in the area was constantly 100% all year round with consistent muddy sand seabed and classified as Jerlov water type I (Jerlov, 1977; Armiyanti et al., 2013; Prawira et al., 2013).

2.2 Data collection

Two field surveys were conducted at the study site. The first field survey was conducted between 17 and 19 March 2010 to determine the reference (control) points and measure seaweed biomass. The second was carried out between 26 and 27 October 2010 to determine accuracy (training) points and measure spectral reflectance of the cultured seaweed. Sampling points were selected using stratified random sampling technique by plotting 1×1 m quadrat randomly along line transects parallel to the shoreline at every 20–50 m to cover different substrates (i.e., seaweed, seagrass, and sand). The coordinates of each point were recorded at the center of the quadrat using a handheld GPS. There were 210 sampling stations selected in the study site with a depth range of 0.8–2.2 m (Fig. 1). In-situ biomass sampling was conducted at 20 selected sampling points using 1×1 m quadrat divided into 25×25 cm subquadrat of intersecting strings for practical reason. Seaweed belonged to any of each subquadrat was randomly collected from the main culture rope and stored in a labeled sealable plastic bag. Each sample was rinsed with clear seawater, drained, and weighed using a digital scale. The sample was then transferred to a new labeled plastic bag for dry weight measurement at the laboratory.

The sampling stations were categorized into two groups, divided alternately between them by chronological order during sampling works. The first group was the reference (control) points which served as the initial points for image classification. The second group was the accuracy (training) points which served as ground-truthing of image classification (Green et al., 2000; Congalton and Green, 2008). The selection of sampling points was adjusted accordingly considering the challenges during sampling activity such as time and resource limitations as well as localized current, weather, tide, and tide patterns (Congalton, 1991; De Gruijter, 1999; Green et al., 2000; McKenzie et al., 2001; Holmes et al., 2006; Olofsson et al., 2014).

The seaweed spectral reflectance was measured using a Spectrometer Ocean Optics type USB2000. The spectral reflectance was measured by pointing the spectrometer probe to the submerged and emerged seaweed colonies at each sampling point. All spectral reflectance measurements were done between 10:30 and 13:30 local time when the sky was clear with no clouds shadow to the seaweed target. The most effective and useful spectral characteristics from this measurement were used in the image classification to distinguish seaweed biomass with other aquatic vegetations. In general, the spectral reflectances of wild and cultivated seaweed were quite similar. The spectral reflectances of seaweed in the visible band with a wavelength range of 350–700 nm were relatively invariable. Higher variations and intensities of seaweed spectral reflectances were observed in the near-infrared (NIR) wavelength range of 700–900 nm (Pratama, 2010; Sagawa et al., 2010). However, penetration limitation of NIR wavelength in the water column was the reason for the ineffective use of NIR in underwater object identification (O'Neill et al., 1987; Holmes et al., 2006; Sagawa et al., 2010; Hamylton, 2011).

2.3 Image dataset

The imagery dataset used in this study was from the Worldview-2 multispectral 8-Band acquisition date of 1 April 2010, commercially distributed in resampled pixel resolution at 2.0 m, geometrically and radiometrically corrected (Level 2A). The Worldview-2 digital numbers were converted to band-averaged spectral radiance ($W \cdot m^{-2} \cdot sr^{-1} \cdot \mu m^{-1}$) and top-of-atmosphere (TOA) reflectance (Updike and Comp, 2010). The TOA reflectances were then atmospherically corrected and converted to surface reflectance using dark object subtraction (DOS) method (Chavez, 1988). The dark signal was acquired from a selected pixel in deep water on the west coast of the study area. The relationship between surface reflectance and seaweed biomass at the sampling points was examined using exponential regression analysis.

The specification of WorldView-2 imagery used in this research is as follows:

Type	: Multispectral 8 Band
Date of acquisition	: 1/04/2010
Time of acquisition (UTC)	: 02:42:05.34 am
Spatial resolution	: 2.0 m
Datum/Projection	: UTM/WGS84
Sun azimuth (deg)	: 63.3
Sun elevation (deg)	: 70.2
Sensor Bands (nm)	: Coastal (400–450); Blue (450–510); Green (510–580); Yellow (585–625); Red (630–690); Red Edge (705–745); Near-IR1 (770–895); Near-IR2 (860–1040)

2.4 Image processing

Supervised classification with maximum likelihood (MLC) and contextual editing (CE) were used in the image processing in combination with and without DII before the image classification process. The image processing procedures consisted of four different methods (Tab. 1), which are method I, II, III, and IV. The first and third methods (I and III) applied supervised classification (MLC) only, while the second and fourth methods (II and IV) applied DII in conjunction with MLC. The combination of five visible bands (coastal, blue, green, yellow, and red) was used in method I and II, while method III and IV used one pair of the most effective visible band as a comparison. All method described uses CE as the subsequent element in the classification process.

DII is a correction technique developed by Lyzenga (1981) to eliminate the influence of water columns on the spectral reflectance of objects received by onboard remote sensing

Table 1. Image processing methods used in this study.

	Method			
	I	II	III	IV
Band combination	5	5	2	2
Classification technique	MLC	DII + MLC	MLC	DII + MLC

Table 2. Combination of bands for depth invariant index image composite.

5 Band pair			
C/B	B/G	G/Y	Y/R
C/G	B/Y	G/R	
C/Y	B/R		
C/R			

C = Coastal (band 1); B = Blue (band 2); G = Green (band 3); Y = Yellow (band 4); R = Red (band 5).

sensors. This method has been widely used in shallow seabed mapping (Watkins, 2015; Manuputty et al., 2017). DII has some advantages over other methods in terms of its simple application and relatively higher accuracy in image spectral transformation through the use of the attenuation coefficient of a particular water body (Lyzenga, 1981; Flener et al., 2010; Zoffoli et al., 2014). The transformation formulation using DII can be expressed as follows:

$$Y_{ij} = X(\lambda)_i - {}^{K_i}/_{K_j} X(\lambda)_j \quad (1)$$

where:

$X(\lambda)_i, X(\lambda)_j$ = The values of spectral transformation of band i and j, determined from:

$$X(\lambda)_i = \ln\left(L(\lambda)_i - L(\lambda)_{\infty i}\right) \quad (2)$$

$L(\lambda)_i$, $L(\lambda)_j$ = Spectral reflectance of band i and j

$L(\lambda)_{\infty i}$, $L(\lambda)_{\infty j}$ = Spectral reflectance of optically deep water in band i and j

${}^{K_i}/_{K_j}$ = Attenuation coefficient of water column in band i and j, determined from:

$${}^{K_i}/_{K_j} = a + \sqrt{(a^2 + 1)} \quad (3)$$

$$a = {}^{(\sigma_i - \sigma_j)}/_{2\sigma_{ij}} \quad (4)$$

σ_i, σ_j = Variance of band i and j

σ_{ij} = Covariance of band i and j.

The basic principle of the DII algorithm for water column correction is the differences of spectral reflectance of different image pixels representing the same substrate feature determined by the water depth variation and the value of the attenuation coefficient. The transformation of images using the DII algorithm produces a new image composite where the pixel values are not the spectral reflectance of the substrate/surface but the values represent the relationship between the two bands' spectral reflectances in which the influences of water depth have been minimized (Lyzenga, 1981; Stumpf et al., 2003; Flener et al., 2010; Zoffoli et al., 2014; Hoang et al., 2015). In this study, visible band pairing in the DII approach creates ten different band pairs in 5-band pairing (Tab. 2) and one band pair in 2-band pairing, with attenuation coefficient ratio derived from atmospherically corrected of transformed reflectance ($X_{(\lambda)}$) values.

The image supervised classification was performed using maximum likelihood (MLC) in conjunction with contextual editing (CE) as the subsequent classification element. The MLC method was used under the assumption that a normal data distribution occurred in each band classification class. The class of classification in each band is a function of pixel mean and variance/covariance values based on reference points dataset (Andréfouët et al., 2003, 2004; Benfield et al., 2007; Richards, 2013). The mathematical model of each pixel in each band classification is as follows:

$$g_i(x) = \ln p(\omega_i) - {}^1/_2 \ln\left|\sum_i\right| - {}^1/_2 (x - m_i)^T \sum_i^{-1} (x - m_i) \quad (5)$$

where:

$g_i(x)$ = Discriminant function

ω_i = Spectral reflectance class, where $i = 1,\ldots M$, and M = number of classes

$p(\omega_i)$ = Probability of selected class ω_i

$|\sum_i|$ = Determinant from class data covariance matrix

x = n-dimension of the data, where n = number of bands

$\sum_i^{-1}$ = Reciprocal matrix

m_i = Average vector.

MLC is a general classification method commonly used in mapping shallow water seabed using high-resolution satellite remote sensing imagery such as WorldView-2. This method can produce a highly accurate classification of underwater objects.

The use of contextual editing (CE) as the subsequent element was done by applying specific limitations in the classification process to consider generic patterns of habitat distribution. Some *a priori* and *a posteriori* contextual rules were used in the reclassification process of this study. Depth and exposure were done automatically (*a priori*) as well as shape and visual interpretation which was done manually (*a posteriori*). Using the *a posteriori* CE approach, misclassification or spectral confusion results were edited/reclassified into the appropriate classification categories. For example, pixels representing a seaweed farmer boat and incorrectly

classified as sands or aquatic vegetations were reclassified into a corresponding class. The combination between MLC and CE can reduce the occurrence of unwanted and miscategorized classes through more specific class codification using spectral classification pattern, value range, and parameter suitability based on the known characteristic of the environment being studied (Mumby et al., 1998; Green et al., 2000; Richards, 2003; Andréfouët et al., 2004; Benfield et al., 2007; Knudby and Nordlund, 2011; Rioja-Nieto et al., 2013).

In the process of image classification, map features in this study were categorized into three distinctive classes which were seaweed, seagrass, and sand. The seaweed category itself was divided into two classes differentiated by the weight group per quadrat area (m^2): Seaweed I for 0.5–1 kg, and Seaweed II for 1–2 kg. The remaining ungrouped features were collectively categorized as "others".

2.5 Accuracy assessment

Image data processing involves two types of accuracy calculations: positional accuracy, and thematic accuracy. Positional accuracy describes how far the distance between the position of objects in a map and the real world. Thematic accuracy shows how accurately the objects are identified in the map (McKenzie et al., 2001; Congalton and Green, 2008). Thematic accuracy consists of two types of accuracy: user accuracy and producer accuracy. User accuracy tells about the probability of a classified image pixel to accurately represent the real objects while producer accuracy indicates the probability that every pixel in an image has been correctly classified. The calculation of thematic accuracy can be done by building a contingency matrix (Congalton and Green, 2008) which includes the overall accuracy, user accuracy, and producer accuracy. The calculation of each accuracy type is presented as follows based on the method suggested by Foody and Atkinson (2002):

$$\text{Producer accuracy (PA)} = \frac{\sum_{i=1}^{k} n_{ii}}{n_{i+}} \tag{6}$$

$$\text{User accuracy (UA)} = \frac{\sum_{i=1}^{k} n_{ii}}{n_{+i}} \tag{7}$$

$$\text{Overall accuracy (OA)} = \frac{\sum_{i=1}^{k} n_{ii}}{N} \tag{8}$$

where:

k = Number of classes

nii = Number of correctly classified classes

n_{+i} = Number of classified observation in i-class in the reference map

n_{i+} = Number of classified observation in i-class on the map

N = Number of observation points.

It is important to note that these accuracy types still have some biases affecting the overall classification result. User accuracy measures the level of omission errors (excluding the areas that should be included in a particular class), producer accuracy measures the level of commission errors (keeping the areas that should be omitted from a particular class), and overall accuracy contains both errors. To determine the successful ratio of accuracy produced by the automated classification process in comparison to reference data, the Tau coefficient was used (Ma and Redmond, 1995; Næsset, 1996; Mumby and Edwards, 2002; Couto, 2003). The Tau coefficient is determined by:

$$T = \frac{P_0 - P_r}{1 - P_r} \tag{9}$$

where:

P_o = overall accuracy

P_r = random agreement based on the number of classes, calculated from:

$$P_r = \frac{1}{N^2} \sum_{i=1}^{M} n_i . x_i \tag{10}$$

M = number of classes/group

i = class/group sequence

N = number of pixels

n_i = number of rows in class/group i

x_i = diagonal values in class/group i.

2.6 Seaweed biomass estimation

After classification and evaluation of its accuracy, the harvest potential of seaweed could be calculated based on the total seaweed farming area produced by the highest accuracy classification method and in-situ measurement of seaweed biomass (density, fresh weight/FW, and dry weight/DW). Biomass here is defined as the total mass of an organism in a given area (Simms, 2003; Barillé et al., 2010; Silva et al., 2010), and can be calculated as follows:

$$B_x = \frac{W_x}{A_q} \tag{11}$$

where:

B_x = Seaweed biomass at sampling point x (g/m^2 DW)

W_x = Seaweed weight at sampling point x (g DW)

A_q = Area of quadrat (m^2).

The estimation of total seaweed biomass at the time of sampling was obtained by multiplying the mean biomass from each seaweed class with the total area of seaweed identified from the image classification process, calculated as follows:

$$B^{\text{mean}} = \frac{1}{N} \sum_{x=1}^{n} B_x \tag{12}$$

$$B^{\text{total}} = B^{\text{mean}} . A^{\text{total}} \tag{13}$$

where:

B^{mean} = Mean seaweed weight of all sampling points (g/m^2 DW)

N = Number of biomass sampling data

B^{total} = Total biomass of identified seaweed class (g DW)

A^{total} = Total all area of identified seaweed class (m^2).

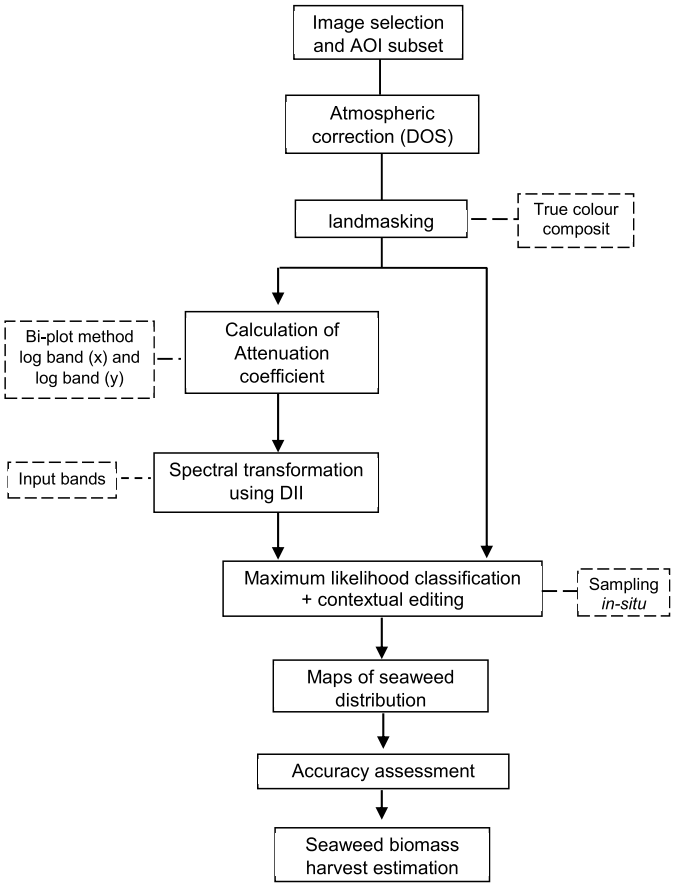

Fig. 2. The research design of seaweed harvest biomass prediction.

The calculation of seaweed biomass prediction was based on Lambert–Beer Law which describes the relationship between light attenuation of a species and its density. Lambert-Beer law states that light absorption is proportional to the thickness of aquatic vegetation pigments and water columns. The spectrum transmission from this process could be used to determine the composition and density of submerged aquatic vegetation with great accuracy (Tucker and Sellers, 1986; Beil et al., 1998; Stekoll et al., 2006; Gitelson et al., 2008; Sekioka et al., 2008; Huesemann et al., 2013).

The research design of this study is provided in Figure 2.

3 Results

3.1 Study area

The vegetation compositions of the study area were dominated by cultured seaweed of *K. alvarezii*. The cultured *K. alvarezii* was submerged at a depth around 0.4–1.2 m and has various age cultures from 1 to 40 days. Seagrass patches from the species of *Thalassia hemprichii*, *Enhalus acoroides*, and *Halophila ovalis* grew on the relatively homogenous sandy substrates.

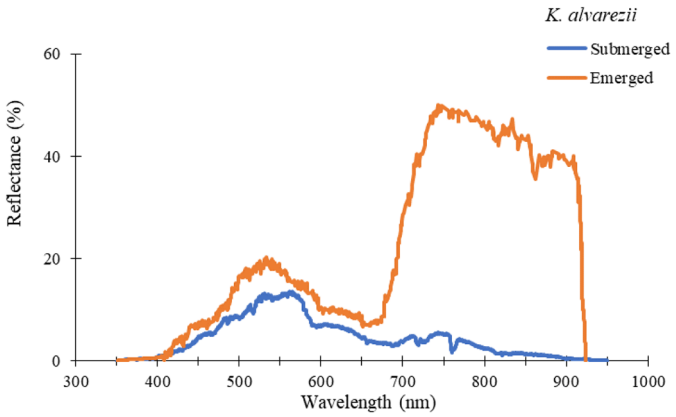

Fig. 3. Spectral reflectances of seaweed *K. alvarezii* measured at submerged and emerged.

3.2 Data collection

The measured spectral reflectances of emerged and submerged seaweed are presented in Figure 3. The highest spectral reflectance measured from above the water surface was within NIR and green bands while submerged spectral reflectance was within blue and green. Due to the limited capability of the NIR band to penetrate the water column, the blue band (450–510 nm) was the most effective, and the green band (510–580 nm) was the second most effective one.

3.3 Image dataset

Mean surface reflectance transformed from the satellite image at the reference points of each band is presented in Figure 4. In this figure, the highest surface reflectance for seaweed, seagrass, and sand were identified within blue and green bands. Three bottom features have different values of surface reflectance signaled from significant differentiation of homogenous pixel for each feature.

3.4 Image processing

Results of the image transformation using four different methods had produced a classification based on different benthic features and the predicted biomass of seaweed *K. alvarezii* as presented in Figure 5. The contextual editing (CE) used to improve the classification process was based on shape and visual interpretation of known objects. CE was used to reclassify wave foam and seaweed farmer boat pixels incorrectly classified as Seaweed, Seagrass, and mostly Sands, into Others category. The predicted seaweed biomass was classified into two classes based on the seaweed dry weight per quadrat area (m2): Seaweed I for 0.5–1 kg, and Seaweed II for 1–2 kg.

3.5 Accuracy assessment

In general, method I has better values on overall accuracy and Tau coefficient, especially on Seaweed II and Seagrass

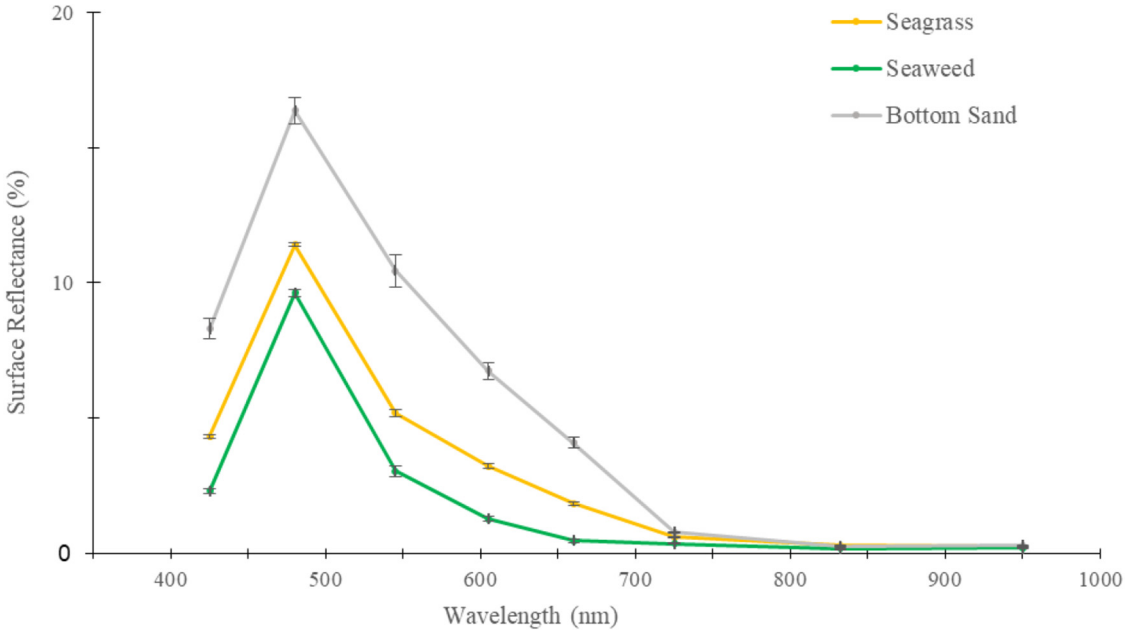

Fig. 4. Mean surface reflectance for three bottom features of Nusa Lembongan beach. Error bars represent ±SE.

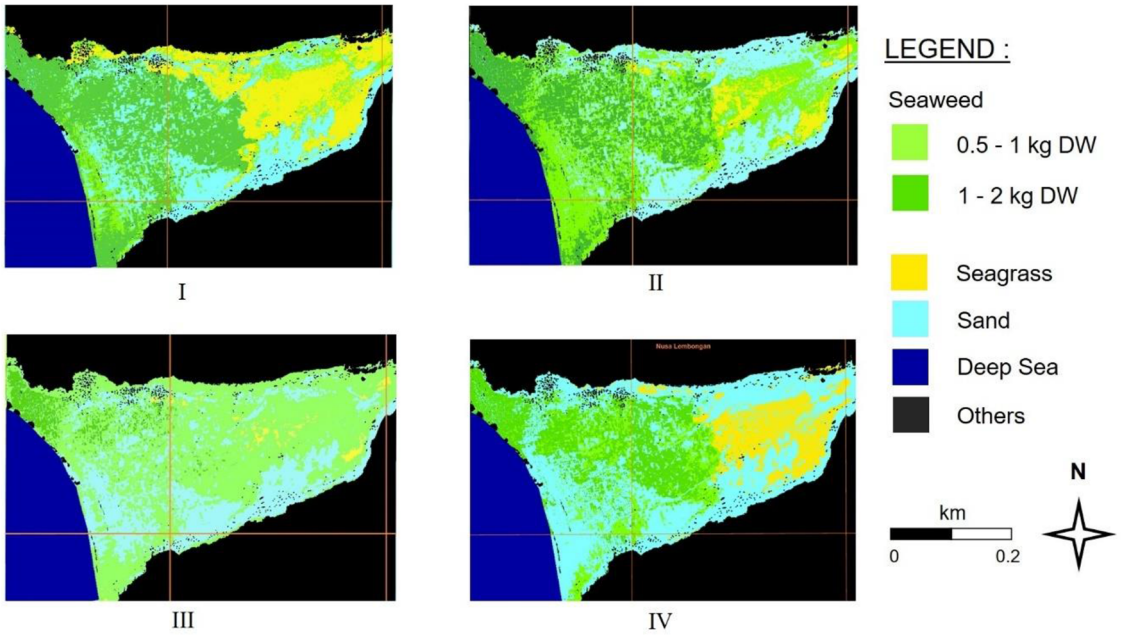

Fig. 5. The results of seaweed classification in Nusa Lembongan: I = 5 bands MLC; II = 5 bands DII and MLC; III = 2 band MLC; IV = 2 band DII and MLC.

classes, than the other three methods (Tab. 3). However, the value of producer accuracy and user accuracy shows that method IV performs slightly better in identifying Seaweed I and Sand classes than the other especially method I. Furthermore, using DII as a correction technique in image processing did improve the classification accuracy while using 2 bands (Blue-Green) as found in method III and IV. Contrastingly, DII did not improve the classification accuracy when using 5 bands as found in method I and II.

The total area of each class produced by the four methods is presented in Table 4. Based on the image classification analysis, method I had the largest coverage of Seaweed II area (0.328 km^2), while method III had the largest coverage of Seaweed I area (0.526 km^2). Considering the achieved accuracy by each method, the total seaweed coverage area resulted from method I was considered as the most accurate and therefore used further to calculate the total seaweed biomass.

Table 3. Seaweed classification accuracy at Nusa Lembongan, Bali.

Method	Classification	PA (%)	UA (%)	OA (%)	TC
I	Seaweed I (1–2 kg)	67.86	79.17	79.05	0.75
MLC 5 Band	Seaweed II (2–4 kg)	91.30	84.00		
	Seagrass	81.48	88.00		
	Sand	72.22	65.00		
	Others	88.89	72.73		
II	Seaweed I (1–2 kg)	68.00	68.00	68.57	0.63
DII+MLC 5 Band	Seaweed II (2–4 kg)	67.74	70.00		
	Seagrass	70.00	70.00		
	Sand	68.42	68.42		
	Others	70.00	63.64		
III	Seaweed I (1–2 kg)	58.62	60.71	58.10	0.52
MLC 2 Band	Seaweed II (2–4 kg)	61.54	57.14		
	Seagrass	52.38	64.71		
	Sand	56.25	50.00		
	Others	61.54	57.14		
IV	Seaweed I (1–2 kg)	74.07	80.00	77.14	0.73
DII+MLC 2 Band	Seaweed II (2–4 kg)	78.57	81.48		
	Seagrass	70.83	68.00		
	Sand	81.25	81.25		
	Others	90.00	75.00		

Table 4. Coverage area of each class from the image classification.

	Coverage (Km^2)			
Class	I	II	III	IV
Seaweed I	0.149	0.372	0.526	0.178
Seaweed II	0.328	0.297	0.137	0.210
Seagrass	0.291	0.119	0.029	0.194
Sand	0.094	0.068	0.163	0.267
Others	0.035	0.041	0.042	0.048
All	0.897	0.897	0.897	0.897

Table 5. Seaweed biomass from in-situ measurement at Nusa Lembongan, Bali.

	Fresh weight (g)	Age (day)	Dry weight (g)	Biomass (g/m^2 DW)
Min	205	1	35	560
Max	900	40	95	1520
Mean±SD	481.25 ± 183.52	17.5 ± 12.43	57.75 ± 17.43	924 ± 278.91

3.6 Seaweed biomass estimation

The average dry weight of each seaweed sample collected during the research was 57.75 ± 17.43 g. Using equation (12), the average calculated biomass per meter square reached 924 ± 278.91 g/m^2 (Tab. 5). The lowest biomass value was 560 g/m^2 for the 1-day cultivated seaweed and the highest was 1520 g/m^2 for seaweed that had been cultivated for 40 days. The average seaweed biomass was 777.14 ± 140.71 g/m^2 for Seaweed I and 1266.67 ± 206.99 g/m^2 for Seaweed II areas (Tab. 6). The total harvestable seaweed biomass (Eq. (13)) was 115.79 ± 20.97 tons for Seaweed I area and 415.47 ± 67.89 tons for Seaweed II area. The total prediction of biomass harvest combined from both classes was 531.26 ± 250.29 tons. The exponential relationship between seaweed spectral reflectance and biomass is presented in Figure 6. The highest relationship

Table 6. Seaweed stock assessment by classes identification.

Class	Biomass (g/m^2 DW)			Stock estimation
	Min	Max	Mean ±SD	(Ton DW)
Seaweed I	560	976	777.14 ±140.71	115.79 ± 20.97
Seaweed II	1024	1520	1266.67 ±206.99	415.47 ± 67.89
Total				**531.26 ± 250.29**

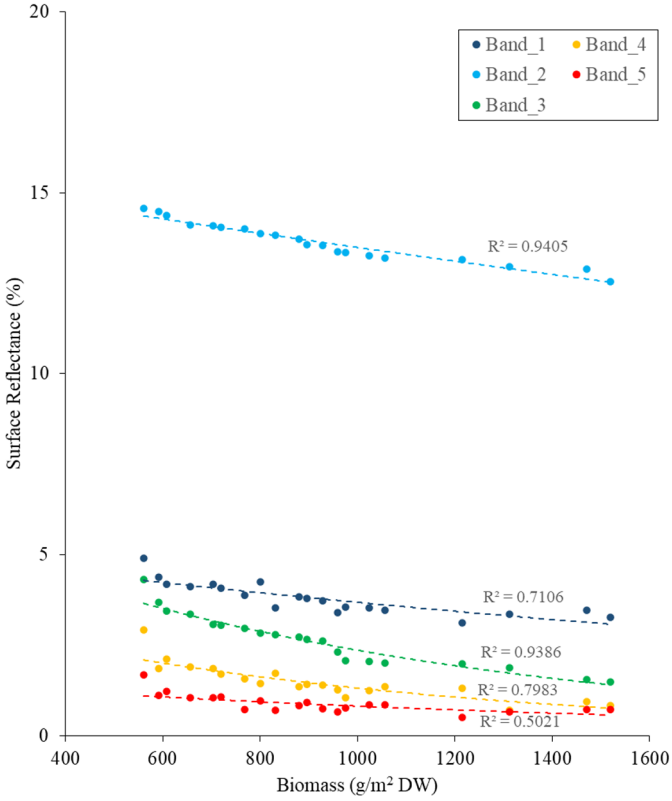

Fig. 6. The relationship between spectral reflectance of different bands and the measured seaweed biomass.

between seaweed biomass and satellite surface reflectance was the blue band with $R^2 = 0.9405$ and green band with $R^2 = 0.9386$.

4 Discussion

The measurement of in-situ spectral reflectance of emerged and submerged seaweed indicated the relatively strong influence of water column and depth in object identification and classification. Results of the in-situ measurements showed that the NIR band has the highest value of spectral reflectance for emerged (above the water surface) but the lowest for submerged (under the water surface) seaweed. Theoretically, the coastal band (band 1) has the highest water column penetration. Thus, the band was supposed to be useful in shallow water mapping. However, spectral characteristics data from field measurements and satellite imagery showed that the blue (band 2) and green (band 3) bands have higher spectral values compared to coastal (band 1). Several other studies observed the dwindling capabilities and poor results of the coastal band in water penetration due to atmospheric and surface noises generated from high scattering and absorption in short wavelengths such as in Manessa et al. (2016a,b), Collings et al. (2018), and Cross et al. (2018). A study by Miecznik and Grabowska (2012) revealed that the coastal band only penetrates deepest in pure water. Furthermore, Stumpf et al. (2003) and Sagawa et al. (2010) confirmed that blue and green bands have better water column penetration than other bands and contain sufficient spectral reflectance to be used in identifying underwater vegetation.

The image processing using 5-band MLC+CE has produced the highest accuracy for the classification map with the OA of 79.05% and TC of 0.75. These values indicated a highly successful classification in coastal areas considering the difficulty of delineating seaweed and seagrass classes in mixed pixel conditions (Foody, 2008). Study at other locations in Indonesia using Landsat-7 by Wouthuyzen et al. (2016), GeoEye-1 by Setyawidati et al. (2018a), and Worldview-2 by Setyawidati et al. (2018b), although resulted in slightly lower accuracy, also reported the capabilities of image classification process to successfully differentiates specific features within brown macroalgae habitat. Cultured seaweed and wild seagrass have a similar reflectance pattern but with different spectral reflectance values (Fig. 4). Both vegetations also have other differences in terms of habitat locations, growth depths, and coverage patterns. For example, the classification map results showed that the coverage pattern of seaweed formed straight lines in rectangular patterns compared to the irregular pattern of seagrass coverage. Seaweed was cultured suspended in the water column (0.5–1 m from the seabed and water surface) compared to seagrass which grows at the seabed. These locational growth differences according to Silva et al. (2008) influence the overall spectral reflectance characteristics of the submerged vegetation.

The high correlation between the spectral reflectance of blue and green bands with the measured biomass indicated a high accuracy which, in turn, can be used to validate the estimation of seaweed harvestable biomass. However, the combination of five bands in the classification process resulted in higher classification accuracy rather than using only two bands of the blue and green spectrum. This result indicates that the coastal (band 1), yellow (band 4), and red (band 5) were useful in the seaweed image classification process as well although they have a lower correlation to biomass than blue and green. Schalles (2006) and Silva et al. (2008) have both argued that biophysical characteristics such as leaf coverage, biomass density, vegetation orientation, and distribution could be determined from the spectral reflectance of the submerged

vegetation. High coverage and horizontal density correspond positively to a spectral reflectance compared to low density and vertical distribution of submerged vegetation. However, the close relationship between vegetation biomass and spectral reflectance occur on certain wavelength and cannot be considered uniform on all wavelengths. The high density and wide coverage of submerged vegetation could have low spectral reflectance due to the spectral characteristics of the wavelength (Louchard et al., 2003; Schalles, 2006; Silva et al., 2008; Castillo-Santiago et al., 2010).

The higher overall accuracy of 5-band MLC than 2-band DII+MLC provides evidence that the DII method was not necessarily useful in improving accuracy when using five bands combination of MLC in image processing for seaweed classification. However, within two-band combinations, the DII+MLC method was useful to remove water column influence on the spectral reflectance of the cultured seaweed and successfully able to differentiate it from other class features. The use of satellite images with high spatial resolution also contributed significantly to the high accuracy of the MLC classification results. These similar results, although performed with different band combinations, have also been confirmed by Setyawidati et al. (2018a,b). Furthermore, Stekoll et al. (2006) reported the overestimation in estimating kelp canopy area using Landsat 7 imagery which corresponds to the low spatial imagery. Overall, the 5-band MLC and 2-band DII+MLC methods have higher accuracy and successfully differentiate mixed seaweed and seagrass from other features compared to the other methods applied in this study.

5 Conclusions

The accompanied in-situ spectral measurement suggested that spectral reflectance of submerged vegetation within the water column was different from the same emerged vegetation. The finding is significant in terms of determining the band combination used in classification and biomass estimation of submerged vegetation, particularly seaweed.

The image processing methods developed in this study, along with group separation in seaweed classification, offers a significant improvement over the estimation of harvest potential of seaweed for better management of seaweed supply chain not only in Indonesia but also worldwide. Furthermore, seaweed culture in Indonesia is conducted consistently throughout the year. Thus, this research considered that the un-synchronized time stamp of satellite imagery with the in-situ measurement poses minimal variation in terms of seaweed growth and culture as they were only ten days in date differences as well as within the same seaweed planting calendar.

It should be noted that since 2015 seaweed farming on the Nusa Lembongan study area has declined considerably due to many factors including the low market price, ice-ice disease, and tourism development throughout the region. In 2016, the price of seaweed per kg dry weight in the Nusa Penida and Nusa Lembongan region reach an all-time low since seaweed farming was first introduced two decades ago. The price was only USD 0.16 per kg for *E. spinosum* and USD 0.39 per kg for *K. alvarezii*. Combined with the increasing prevalence of ice-ice disease, these situations prompt the seaweed farmers, especially young people, to pursue other alternative means to make a living. Their shift to other jobs was mostly to tourism sectors as an obvious choice in this region which has been increasing rapidly since 2011 (Keohane, 2016; Anonymous, 2019; Andréfouët et al., 2021). Nevertheless, this study can still provide good baseline information when the seaweed industry in this area was still in a good state and for other seaweed cultivation areas that remain active as well.

Recently, a report by ABC News Australia in March 2021 titled "The Year Bali Tourism Stopped" describes the tourism in Nusa Lembongan is in suspended animation due to the COVID-19 pandemic. The report specifies that seaweed farming in Nusa Lembongan that was once replaced by tourism has found its footing again and helped the local communities to get back on their feet (Davis, 2021). This new development means that the information provided by this study could aid local and national governments to seek market destinations of potential large seaweed harvest from this area.

Acknowledgement. This research was supported by the 2010 Research Fund (DIPA) of the Ministry of Fisheries and Marine Affairs. We are very grateful to Dr. Aryo Hanggono, Iqbal Suhaemi Gultom, Sundari Wening Warastri, and I Wayan Suarbawa for providing research support and assistance.

References

Ackleson SG, Klemas V. 1987. Remote sensing of submerged aquatic vegetation in lower Chesapeake Bay: a comparison of Landsat MSS to TM imagery. *Remote Sens Environ* 22: 235–248.

Andréfouët S, Kramer P, Torres-Pulliza D, Joyce KE, Hochberg EJ, Garza-Pérez R, Mumby PJ, Riegl B, Yamano H, White WH, Zubia M. 2003. Multi-site evaluation of IKONOS data for classification of tropical coral reef environments. *Remote Sens Environ* 88: 128–143.

Andréfouët S, Zubia M, Payri C. 2004. Mapping and biomass estimation of the invasive brown algae *Turbinaria ornata* (Turner) J. Agardh and *Sargassum mangarevense* (Grunow) Setchell on heterogeneous Tahitian coral reefs using 4-meter resolution IKONOS satellite data. *Coral Reefs* 23: 26–38.

Andréfouët S, Payri C, Van Wynsberge S, Lauret O, Alefaio S, Preston G, Yamano H, Baudel S. 2017. The timing and the scale of the proliferation of Sargassum polycystum in Funafuti Atoll, Tuvalu. *J Appl Phycol* 29: 3097–3108.

Andréfouët S, Subky B, Gaspar P, Farhan AR. 2018. INDESO project: results from application of remote sensing and numerical models for the monitoring and management of Indonesia coasts and seas. *Mar Pollut Bull* 131: 1–6.

Andréfouët S, Dewantama IMI, Ampou EE. 2021. Seaweed farming collapse and fast changing socio-ecosystems exacerbated by tourism and natural hazards in Indonesia: a view from space and from the households of Nusa Lembongan island. *Ocean Coast Manage* 207: 105586.

Anggadiredja JT, Zatnika A, Purwoto H, Istini S. Seaweed (*Rumput Laut*). Penebar Swadaya, Jakarta, 2006 (in Indonesian).

Anonymous. Movement Seaweed Farmer in Nusa Lembongan. Wisnu Foundation, 2019. Retrieved March 2, 2020 from http://www.wisnu.or.id/2019/12/11/movement-seaweed-farmer-in-nusa-lembongan

Armiyanti NPNN, Sutarjo, Surata IK. 2013. Productivity of seaweed farming in coastal waters of Nusa Penida, Klungkung Regency

(*Tingkat Produktivitas Budidaya Rumput Laut Pada Perairan Pantai Di Kecamatan Nusa Penida Kabupaten Klungkung*). *J Pendidik Geogr Undiksha* 3 (in Indonesian).

Barillé L, Robin M, Harin N, Bargain A, Launeau P. 2010. Increase in seagrass distribution at Bourgneuf Bay (France) detected by spatial remote sensing. *Aquat Bot* 92: 185–194.

Beil A, Daum R, Harig R, Matz G. Remote sensing of atmospheric pollution by passive FTIR spectrometry, in Spectroscopic Atmospheric Environmental Monitoring Techniques, Vol. 3493. International Society for Optics and Photonics, 1998, pp. 32–44.

Benfield SL, Guzman HM, Mair JM, Young JAT. 2007. Mapping the distribution of coral reefs and associated sublittoral habitats in Pacific Panama: a comparison of optical satellite sensors and classification methodologies. *Int J Remote Sens* 28: 5047–5070.

Castillo-Santiago MA, Ricker M, de Jong BH. 2010. Estimation of tropical forest structure from SPOT-5 satellite images. *Int J Remote Sens* 31: 2767–2782.

Chavez PS. 1988. An improved dark-object subtraction technique for atmospheric scattering correction of multispectral data. *Remote Sens Environ* 24: 459–479.

Collings S, Botha EJ, Anstee J, Campbell N. 2018. Depth from satellite images: depth retrieval using a stereo and radiative transfer-based hybrid method. *Remote Sens* 10: 1247.

Congalton RG. 1991. A review of assessing the accuracy of classifications of remotely sensed data. *Remote Sens Environ* 37: 35–46.

Congalton RG, Green K. Assessing the Accuracy of Remotely Sensed Data: Principles and Practices, 2nd ed., CRC Press/Taylor and Francis Group, 2008.

Couto P. 2003. Assessing the accuracy of spatial simulation models. *Ecol Modell* 167: 181–198.

Cross MD, Scambos TA, Pacifici F, Marshall WE. 2018. Validating the use of metre-scale multi-spectral satellite image data for identifying tropical forest tree species. *Int J Remote Sens* 39: 3723–3752.

Davis M. 2021. The year Bali tourism stopped. *ABC News*. Retrieved March 30, 2020 from https://www.abc.net.au/news/2021-03-09/bali-return-of-seaweed-farming-ceningan-lembongan-penida-covid/13202170

De Gruijter J. Spatial sampling schemes for remote sensing, in Spatial Statistics for Remote Sensing, Springer, Dordrecht, 1999, pp. 211–242.

FAO. The state of world fisheries and aquaculture. Food and Agriculture Organization of the United Nations, Rome, 2014.

FAO. The State of World Fisheries and Aquaculture – Meeting the sustainable development goals. Food and Agriculture Organization of the United Nations, Rome, 2018.

Flener C, Lotsari E, Alho P, Käyhkö J. 2010. Comparison of empirical and theoretical remote sensing-based bathymetry models in river environments. *River Res Appl* 28, 118–133.

Foody GM, Atkinson PM. Uncertainty in remote sensing and GIS. John Wiley and Sons, 2002.

Foody GM. 2008. Harshness in image classification accuracy assessment. *Int J Remote Sens* 29: 3137–3158.

Gitelson AA, Dall'Olmo G, Moses W, Rundquist DC, Barrow T, Fisher TR, Gurlin D, Holz J. 2008. A simple semi-analytical model for remote estimation of chlorophyll-a in turbid waters: Validation. *Remote Sens Environ* 112: 3582–3593.

Green E, Mumby P, Edwards A, Clark C. Remote Sensing: Handbook for Tropical Coastal Management. United Nations Educational, Scientific and Cultural Organization (UNESCO), 2000.

Hamylton S. 2011. An evaluation of waveband pairs for water column correction using band ratio methods for seabed mapping in the Seychelles. *Int J Remote Sens* 32: 9185–9195.

Hoang TC, O'Leary MJ, Fotedar RK. 2015. Remote-sensed mapping of *Sargassum* spp. Distribution around Rottnest Island, Western Australia, using high-spatial resolution WorldView-2 satellite data. *J Coast Res* 32: 1310–1321.

Holmes KW, Van Niel K, Kendrick G, Baxter K. Designs for remote sampling: review, discussion, examples of sampling methods and layout of scaling issues. Technical report, Cooperative Research Centre for Coastal Zone, Estuary and Waterway Management, Australia, 2006.

Huesemann MH, Van Wagenen J, Miller T, Chavis A, Hobbs S, Crowe B. 2013. A screening model to predict microalgae biomass growth in photobioreactors and raceway ponds. *Biotechnol Bioeng* 110: 1583–1594.

Jerlov NG. 1977. Classification of seawater in terms of quanta irradiance. *ICES J Mar Sci* 37: 281–287.

Kanno A, Tanaka Y. 2012. Modified Lyzenga's method for estimating generalized coefficients of satellite-based predictor of shallow water depth. *IEEE Geosci Remote Sens Lett* 9: 715–719.

Keohane A. A Look Into the Carrageenan Industry: How Tourism, Markets and Demand Affect the Seaweed Farmers of Bali Indonesia. Center for Marine Biodiversity and Conservation, San Diego, 2016.

Knudby A, Nordlund L. 2011. Remote sensing of seagrasses in a patchy multi-species environment. *Int J Remote Sens* 32: 2227–2244.

Louchard EM, Reid RP, Stephens FC, Davis CO, Leathers RA, Valerie DT. 2003. Optical remote sensing of benthic habitats and bathymetry in coastal environments at Lee Stocking Island, Bahamas: a comparative spectral classification approach. *Limnol Oceanogr* 48: 511–521.

Lyzenga DR. 1981. Remote sensing of bottom reflectance and water attenuation parameters in shallow water using aircraft and Landsat data. *Int J Remote Sens* 2: 71–82.

Ma Z, Redmond RL. 1995. Tau coefficients for accuracy assessment of classification of remote sensing data. *Photogramm Eng Remote Sens* 61: 435–439.

Manessa MDM, Kanno A, Sekine M, Haidar M, Yamamoto K, Imai T, Higuchi T. 2016a. Satellite-derived bathymetry using Random Forest Algorithm and WorldView-2 imagery. *Geoplanning: J Geomat Plan* 3: 117–126.

Manessa MDM, Haidar M, Budhiman S, Winarso G, Kanno A, Sagawa T, Sekine M. 2016b. Evaluating the performance of Lyzenga's water column correction in case-1 coral reef water using a simulated WorldView-2 imagery. *IOP Conf Ser: Earth Environ Sci* 47: 012018.

Manuputty A, Gaol JL, Agus SB, Nurjaya IW. The utilization of depth invariant index and principle component analysis for mapping seagrass ecosystem of Kotok Island and Karang Bongkok, Indonesia, in IOP Conference Series: Earth and Environmental Science, IOP Publishing, 2017.

McKenzie LJ, Finkbeiner MA, Kirkman H. Methods for mapping seagrass distribution. Global Seagrass Research Methods. Elsevier B.V., 2001, pp. 101–121.

Miecznik G, Grabowska D. WorldView-2 bathymetric capabilities, in Proceeding SPIE 8390: *Algorithms and Technologies for Multispectral, Hyperspectral, and Ultraspectral Imagery XVIII*, 2012.

Ministry of Marine Affairs and Fisheries (MMAF). Indonesian Aquaculture Statistics 2014. Ministry of Marine Affairs and Fisheries, Republic of Indonesia, Jakarta, 2015.

Ministry of Marine Affairs and Fisheries (MMAF). Yearly Report of 2018. Ministry of Marine Affairs and Fisheries, Jakarta, 2019.

Mulyati H, Geldermann J. 2017. Managing risks in the Indonesian seaweed supply chain. *Clean Technol Environ Policy* 19: 175–189.

Mumby PJ, Clark CD, Green EP, Edwards AJ. 1998. Benefits of water column correction and contextual editing for mapping coral reefs. *Int J Remote Sens* 19: 203–210.

Mumby PJ, Edwards AJ. 2002. Mapping marine environments with IKONOS imagery: enhanced spatial resolution can deliver greater thematic accuracy. *Remote Sens Environ* 82: 248–257.

Næsset E. 1996. Conditional tau coefficient for assessment of producer's accuracy of classified remotely sensed data. *ISPRS J Photogramm Remote Sens* 51: 91–98.

O'Neill NT, Kalinauskas AR, Borstad GA, Edel H, Gower JF, Vander Piepen H. Imaging spectrometry for water applications, in Proceeding SPIE 0834, Imaging Spectroscopy II, 1987, pp. 129–136.

Olofsson P, Foody GM, Herold M, Stehman SV, Woodcock CE, Wulder MA. 2014. Good practices for estimating area and assessing accuracy of land change. *Remote Sens Environ* 148: 42–57.

Perryman SE, Lapong I, Mustafa A, Sabang R, Rimmer MA. 2017. Potential of metal contamination to affect the food safety of seaweed (*Caulerpa* spp.) cultured in coastal ponds in Sulawesi, Indonesia. *Aquac Rep* 5: 27–33.

Pratama I. Preliminary study of the use of remote sensing in the identification and mapping of seaweed farming (*Kajian Awal Penerapan Teknologi Penginderaan Jauh Dalam Identifikasi dan Pemetaan Rumput Laut Untuk Perencanaan Dan Pengembangan Kawasan Budidaya Rumput Laut*). Pemanfaatan Teknologi Untuk Kesejahteraan Masyarakat Pesisir. Pusat Riset Teknologi Kelautan, Jakarta, 2010 (in Indonesian).

Prawira MO, Riyantini I, Kurniawati N. 2013. The characteristic dynamics of seagrass bioecology in Nusa Lembongan, Bali Province (*Dinamika Karakteristik Bioekologi Lamun Di Nusa Lembongan Provinsi Bali*). *J Perikan Kelaut* 4: 393–402. (in Indonesian).

Richards JA. Remote Sensing Digital Image Analysis, An Introduction, Vol. XIX, 5th ed., Springer-Verlag, Berlin Heidelberg, 2013, p. 494.

Rioja-Nieto R, Barrera-Falcón E, Hinojosa-Arango G, Riosmena-Rodríguez R. 2013. Benthic habitat β-diversity modeling and landscape metrics for the selection of priority conservation areas using a systematic approach: Magdalena Bay, Mexico, as a case study. *Ocean Coast Manage* 82: 95–103.

Sagawa T, Boisnier E, Komatsu T, Mustapha KB, Hattour A, Kosaka N, Miyazaki S. 2010. Using bottom surface reflectance to map coastal marine areas: a new application method for Lyzenga's model. *Int J Remote Sens* 31: 3051–3064.

Sarinah S, Djatna T. 2015. Assessment of risk mitigation plan by seaweed industry on seaweed raw material shortage: a study case in South Sulawesi, Indonesia (*Analisis strategi penanganan risiko kekurangan pasokan pada industri pengolahan rumput laut: kasus di Sulawesi Selatan*). *Agritech* 35: 223–233. (in Indonesian with English abstract).

Schalles JF. Optical remote sensing techniques to estimate phytoplankton chlorophyll-a concentrations in coastal, in Remote sensing of aquatic coastal ecosystem processes. Springer, Dordrecht, 2006, pp. 27–79.

Sekioka SI, Ishikawa D, Noro T, Ishiguro E. 2008. Fundamental study on estimation of standing seaweed biomass by remote sensing. *J Remote Sens Soc Jpn* 28: 342–349.

Sievanen L, Crawford B, Pollnac R, Lowe C. 2005. Weeding through assumptions of livelihood approaches in ICM: seaweed farming in the Philippines and Indonesia. *Ocean Coast Manag* 48: 297–313.

Silva TSF, Costa MPF, Melack JM, Novo EMLM. 2008. Remote sensing of aquatic vegetation: theory and applications. *Environ Monit Assess* 140: 131–145.

Silva TSF, Costa MPF, Melack JM. 2010. Assessment of two biomass estimation methods for aquatic vegetation growing on the Amazon Floodplain. *Aquat Bot* 92: 161–167.

Simms ÉL. Submerged kelp biomass assessment using CASI, in Coastal and Marine Geo-Information Systems, Springer, Dordrecht, 2003, pp. 501–509.

Setyawidati N, Liabot PO, Perrot T, Radiarta N, Deslandes E, Bourgougnon N, Rossi N, Stiger-Pouvreau V. 2017. In situ variability of carrageenan content and biomass in the cultivated red macroalga *Kappaphycus alvarezii* with an estimation of its carrageenan stock at the scale of the Malasoro Bay (Indonesia) using satellite image processing. *J Appl Phycol* 29: 2307–2321.

Setyawidati N, Kaimuddin AH, Wati IP, Helmi M, Widowati I, Rossi N, Liabot PO, Stiger-Pouvreau V. 2018a. Percentage cover, biomass, distribution, and potential habitat mapping of natural macroalgae, based on high-resolution satellite data and in situ monitoring, at Libukang Island, Malasoro Bay, Indonesia. *J Appl Phycol* 30: 159–171.

Setyawidati N, Puspita M, Kaimuddin AH, Widowati I, Deslandes E, Bourgougnon N, Stiger-Pouvreau V. 2018b. Seasonal biomass and alginate stock assessment of three abundant genera of brown macroalgae using multispectral high-resolution satellite remote sensing: a case study at Ekas Bay (Lombok, Indonesia). *Mar Pollut Bull* 131: 40–48.

Stekoll MS, Deysher LE, Hess M. 2006. A remote sensing approach to estimating harvestable kelp biomass. *J Appl Phycol* 18: 323–334.

Stumpf RP, Holderied K, Sinclair M. 2003. Determination of water depth with high-resolution satellite imagery over variable bottom types. *Limnol Oceanogr* 48: 547–556.

Sulistijo MS. Research of seaweed cultivation in Indonesia (*Penelitian Budidaya Rumput Laut (Alga Makro/Seaweed) di Indonesia*). Pusat Penelitian Oseanografi Lembaga Ilmu Pengetahuan Indonesia, Jakarta, 2002 (in Indonesian).

Tassan S. 1996. Modified Lyzenga's method for macroalgae detection in water with non-uniform composition. *Int J Remote Sens* 17: 1601–1607.

Tucker CJ, Sellers PJ. 1986. Satellite remote sensing of primary production. *Int J Remote Sens* 7: 1395–1416.

Updike T, Comp C. Radiometric use of WorldView-2 imagery. Technical Note, DigitalGlobe, Inc., 2010, pp. 1–17.

Watkins RL. A Methodology for Classification of Benthic Features using WorldView-2 Imagery. Report prepared for the Ecospatial Information Team, Coral Reef Ecosystem Division, Pacific Islands Fisheries Science Center, Honolulu, HI, 2015, 29 pp, under NOAA contract number WE-133F-15-SE-0518. ftp://ftp.soest.hawaii.edu/pibhmc/website/webdocs/documentation/Classification_of_Benthic_Features_using_WorldView_final.pdf

Wouthuyzen S, Herandarudewi SM, Komatsu T. 2016. Stock assessment of brown seaweeds (Phaeophyceae) along the Bitung-Bentena Coast, North Sulawesi Province, Indonesia for

alginate product using satellite remote sensing. *Procedia Environ Sci* 33: 553–561.

Wright EC. The Upshot of Upgrading: Seaweed Farming and Value Chain Development in Indonesia. University of Hawai'i at Manoa, ProQuest Dissertations Publishing, 2017.

Zamroni A, Yamao M. 2011. Coastal resource management: fishermen-s perceptions of seaweed farming in Indonesia. *Int J Nutr Food Eng* 5: 856–862.

Zoffoli ML, Frouin R, Kampel M. 2014. Water column correction for coral reef studies by remote sensing. *Sensors* 14: 16881–16931.

Cite this article as: Pratama I, Albasri H. 2021. Mapping and estimating harvest potential of seaweed culture using Worldview-2 Satellite images: a case study in Nusa Lembongan, Bali – Indonesia. *Aquat. Living Resour.* 34: 15